ScieRxiv
NOT PEER-REVIEWED
Mini Review

From structural mechanisms to functional design in hard carbon anodes for sodium-ion batteries

Pengcheng Xue[1,2], Hengyuan Hu[1,2], Yuankai Huang[1,2], Yuting Wu[1,2], Zeng Chen[1,2], Ziyan Zeng[1,2], Xingyuan Zhong[1,2], Meisheng Han[1,2,*]

[1]Shenzhen Key Laboratory of Advanced Energy Storage, Department of Mechanical and Energy Engineering, Southern University of Science and Technology, Shenzhen 518055, Guangzhou, China.
[2]SUSTech Energy Institute for Carbon Neutrality, Southern University of Science and Technology, Shenzhen 518055, Guangzhou, China.

[*]**Correspondence to:** Dr. Meisheng Han, Shenzhen Key Laboratory of Advanced Energy Storage, Department of Mechanical and Energy Engineering, Southern University of Science and Technology, Shenzhen 518055, Guangzhou, China. Email: hanms@sustech.edu.cn

Received: 13 October 2026 | Approved: 04 November 2026 | Online: 04 November 2026

Abstract

Hard carbon offers reversible sodium storage at low potentials, making it a promising anode for high-energy sodium-ion batteries. Its capacity depends on both the storage sites formed during carbonization and their reversible use during cycling. This review connects these processes through electrochemically accessible storage space, defined as the sites sodium can reach, occupy and vacate reversibly within a given electrolyte, potential window and cycling time. State-resolved measurements and calculations link pore filling to low-potential capacity, while interlayer participation and transport limitations vary with material and storage conditions. Comparing functional designs separates improved use of hard-carbon sites from additional reaction capacity and altered

© The Author(s) 2026. Open Access This article is licensed under a Creative Commons Attribution 4.0 International License (https://creativecommons.org/licenses/by/4.0/), which permits unrestricted use, sharing, adaptation, distribution and reproduction in any medium or format, for any purpose, even commercially, as long as you give appropriate credit to the original author(s) and the source, provide a link to the Creative Commons license, and indicate if changes were made.

interfacial processes. Their value depends on whether these gains persist after accounting for irreversible sodium loss, added electrode mass and operating potential. Machine-learning-assisted carbonization already supports process selection within tested material systems, whereas atomistic models provide local interpretations for experimental evaluation. Future progress requires descriptors that distinguish site formation from reversible utilization, full-cell comparisons that establish the benefits and costs of functional modification, and traceable datasets for testing model-guided experimental choices. This approach links structural evidence to designs that balance capacity, initial Coulombic efficiency, rate capability and manufacturing demands.

Keywords: Sodium-ion batteries, hard carbon, pore filling, functional composites, machine learning

INTRODUCTION

The growth of renewable energy and electric transport has made raw-material availability, battery cost and service life increasingly important. Sodium is widely available, and some sodium-ion chemistries also use abundant elements such as iron and manganese. Manufacturing can draw on the experience gained from lithium-ion battery production. These advantages make sodium-ion batteries attractive for stationary storage and cost-sensitive transport, while broadening the choice of battery chemistries[1-2]. Turning resource availability into affordable cells also depends on electrode combinations, energy density and manufacturing efficiency.

Energy density is a key link between abundant resources and lower cell costs. Low energy density increases the amounts of active material, current collectors and electrolyte needed for each unit of stored energy. This additional material demand can offset savings in raw-material prices. Yao and colleagues assessed competitiveness through material performance, engineering choices and supply-chain scenarios. Their analysis identified higher energy density as an important way to reduce material requirements per unit of stored energy[1]. Capacity utilization and active-sodium losses therefore shape both electrochemical performance and cell economics.

The negative electrode plays a central role in this performance-cost relationship. Direct sodium storage in graphite is limited partly by sodium-carbon binding energetics, making

ionic size only one consideration. Using graphite-based lithium-ion designs in sodium-ion systems therefore requires reassessing how sodium is stored[3]. Hard carbon offers short-range ordered layers, defects and nanopores as distinct sodium-storage environments. With the same positive electrode, a lower negative-electrode operating potential raises the full-cell voltage [Figure 1a][4-5]. All negative-electrode potentials here are referenced to Na^+/Na; full-cell voltage denotes the potential difference between the two electrodes. Biomass and polymer precursors further broaden feedstock choices and opportunities for structural design[6-7].

Improving hard carbon requires balancing several performance metrics that are closely linked. Exposed surfaces and defects can provide storage sites while promoting solid electrolyte interphase (SEI) formation and irreversible sodium consumption. Initial Coulombic efficiency (ICE) is the first desodiation capacity divided by the first sodiation capacity. It matters especially in full cells, where the sodium inventory is finite[8]. Internal pores provide storage space, while entry pathways, connectivity and filling kinetics determine how much of that space is used [Figure 1b]. Storage near the sodium-deposition potential makes control of polarization during fast charging particularly important[9-10]. Optimizing pore volume and plateau potential therefore requires balancing capacity, efficiency and the potential margin before plating.

Precursor chemistry and carbonization shape the structural environments available for sodium storage in hard carbon[11-13]. Electrochemically accessible storage space describes the sites sodium can reach, occupy and vacate reversibly within a given electrolyte, potential window and cycling time. The distinction between forming sites and using them guides the comparison of precursor control, storage mechanisms and functional modification. Pore volume establishes a structural opportunity; state-resolved measurements show how that opportunity contributes to capacity. Conductive networks, active phases and interfacial layers then address different sources of capacity or polarization. Machine-learning-assisted carbonization and local storage models support the selection and interpretation of these designs. Their evaluation brings reversible utilization together with sodium loss, operating potential and electrode mass, linking the material-level choices in Figure 1c to full-cell performance. Artificial intelligence (AI) supports these choices through defined prediction and experimental-validation tasks.

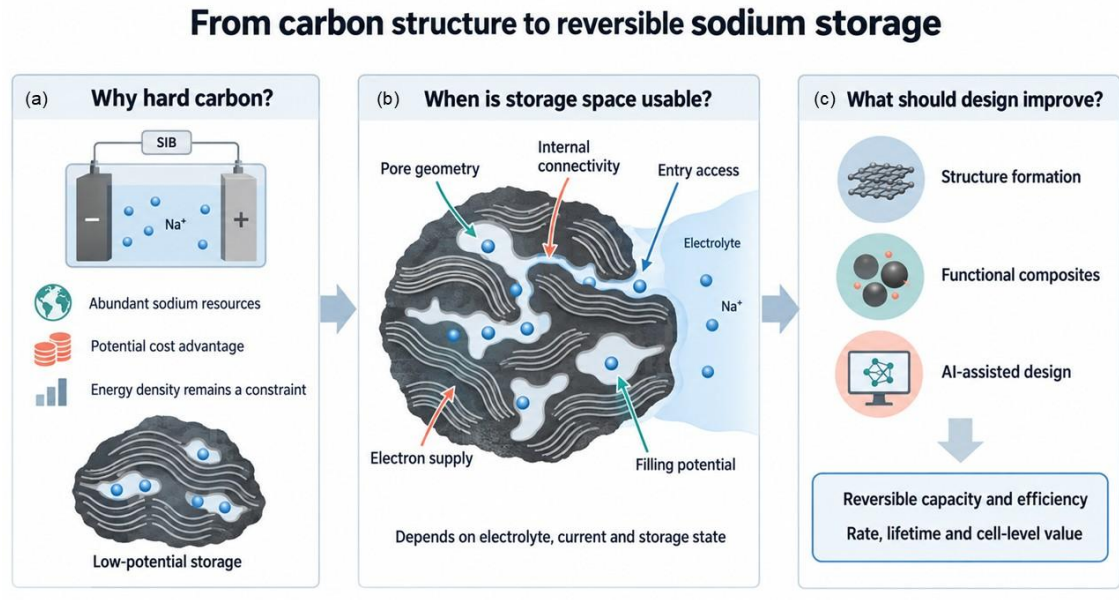


Figure 1. Design questions for hard-carbon anodes in sodium-ion batteries (SIBs). a, Resource and application needs motivate low-potential storage; b, Pore geometry, entry access, internal connectivity, electron supply and filling potential jointly affect utilization; c, Structural control, functional composites and design assisted by artificial intelligence (AI) address capacity, efficiency, rate performance, lifetime and cell-level value. Arrows in this conceptual schematic connect design routes and performance objectives[1,4,8-9].

STRUCTURE FORMATION AND EVIDENCE BASE

Precursors and thermal history jointly shape structure

Precursors supply carbon and shape crosslinking, volatile release and structural rearrangement during processing. Lin and colleagues condensed resorcinol with cinnamaldehyde to form a sterically hindered resin precursor (RFSH). Its styryl groups distinguish it from the resorcinol-formaldehyde resin control (RF) [Figure 2a]. Simulations indicate greater precursor free volume in RFSH [Figure 2b]. After carbonization, the small-angle X-ray scattering (SAXS) profiles differ in shape [Figure 2c]. Together with high-resolution transmission electron microscopy, these differences support more extensive closed-pore formation in the RFSH-derived carbon[6]. Calculated precursor free volume and final pore volume describe different stages of structural evolution. Waste-wood studies associate closed-pore formation with the distinct effects of cellulose and amorphous components on carbon-layer growth[14]. Partial delignification of bamboo links radical evolution to pore formation, while storage performance depends on the extent of treatment[15].

Processing offers several ways to guide structural evolution during hard-carbon formation. Molecular stitching of starch, hydrothermal pretreatment and transient sintering respectively modify chain connections, precursor state and thermal history[7,16-17]. Liquid-phase spatial confinement and disruption of dense coal precursors offer further routes to pore formation. These routes intervene at different stages of carbon formation, so precursor identity alone is an incomplete basis for comparing their final structures[18-19]. Structural comparisons should therefore include pretreatment, heating rate, dwell time and yield alongside precursor identity and peak carbonization temperature.

From geometric pores to usable space

Whether a pore is described as closed depends on how accessibility is measured. Pore geometry describes the dimensions and arrangement of voids, while measured pore volume also depends on access by the chosen probe. Electrochemical accessibility concerns reversible sodium use of these sites within a specified potential window and cycling time; sodium storage requires a pathway connecting the void to ion transport. Carbon-molecular-sieve studies link pore entrances, solvation and interphase formation, indicating that restricted solvent entry can protect internal sites. Their closed-pore criteria apply to the particular ester electrolyte examined[20]. Jin and colleagues compared directly annealed hard carbon (ISO-HC) with hard carbon containing interconnected closed pores (ICP-HC). The latter was prepared by oxidation followed by annealing. Stronger scattering at low scattering-vector magnitude q and a pair-distance distribution shifted toward larger distances support pore expansion in ICP-HC [Figure 2d]. Scattering-based reconstruction yields more expanded, fused pore bodies [Figure 2e]. The authors interpret these results, together with local characterization, as evidence for two structural pathways [Figure 2f]. They propose that direct annealing favors pore isolation, whereas carbon-layer reconfiguration after oxidative pretreatment promotes internally connected pores[9].

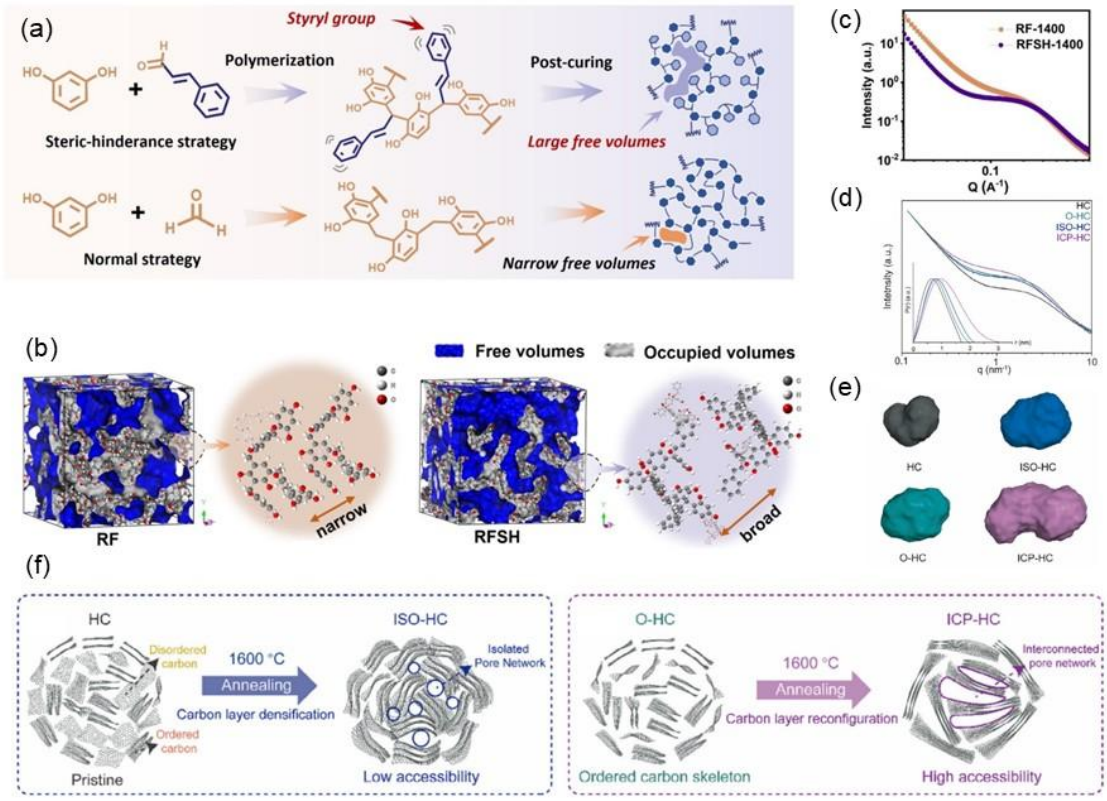


Figure 2. Precursor chemistry and internal-pore formation. a, Polymer synthesis; b, Calculated precursor free volumes; c, Post-carbonization small-angle X-ray scattering (SAXS) evidence. RF and RFSH denote resorcinol-formaldehyde and sterically hindered resorcinol-cinnamaldehyde resin precursors, respectively[6]; d, SAXS and pair-distance distributions; e, Pore-shape reconstruction from scattering models; f, Proposed pore-evolution routes. HC, O-HC and ISO-HC denote the parent, oxidized and directly annealed hard carbons, respectively. ICP-HC denotes hard carbon with interconnected closed pores[9]. Panels a-c and d-f show the materials and evidence from two separate studies.

Accessible storage space can be assessed through pore size and volume, entry access, internal connectivity, electron supply and filling potential[4,8-9]. Electron supply involves both electrode-network transport and local charge compensation, which require measurements appropriate to their respective scales. Jin and colleagues linked pore morphology and scattering after sodiation with capacity. Their treatment also changed the carbon framework and filling potential, so several structural changes could contribute to the improvement[9]. Testing the contribution of connectivity requires comparisons at matched pore volume, framework structure and interfacial conditions. Plateau utilization

across cycling times then tests whether the available space remains usable as current increases.

Complementary observations constrain storage interpretations

Connecting pore structure with reversible capacity requires observations of both the carbon framework and the sodium occupying it. X-ray diffraction (XRD) and Raman spectroscopy constrain average responses of carbon layers or bonding environments. SAXS probes electron-density contrast between pores and the surrounding carbon framework. Pair-distribution-function analysis combined with solid-state nuclear magnetic resonance (NMR) connects local carbon structure with sodium environments[21]. Earlier local-probe studies and NMR combined with density functional theory (DFT) established a basis for analyzing sodium states. Electron paramagnetic resonance adds evidence on spin-related electronic states[22-24].

Interpreting these measurements requires attention to the part of the material each technique can observe. Gas adsorption depends on probe access, whereas microscopy mainly samples local regions. A scattering decrease needs complementary evidence to identify pore filling, and stable average peaks may coexist with small local changes[5,9]. Tracking potential, structure and sodium environments within the same sample allows mechanistic comparisons, including changes that reverse during desodiation. The resulting comparison tests which structural changes accompany sodium uptake and reverse on removal, providing the basis for assigning the storage contributions discussed below.

STORAGE MECHANISMS AND STATE-DEPENDENT KINETICS

Voltage regions and first-cycle sodium losses

Current models describe sodium storage through adsorption at defects and edges, interlayer storage and pore filling[25]. Their relative contributions require interpretation alongside structural and local sodium measurements. Sodiation profiles commonly show a higher-potential slope and a lower-potential plateau, with the boundary defined within each study. In Eren and colleagues' galvanostatic profiles, low-potential plateau capacity decreases markedly at higher current [Figure 3a]. Their scan-rate analysis supports rapid capacitive storage in the sloping region; distributed defect and edge environments

support an adsorption contribution[5]. Identifying atomistic adsorption pathways requires complementary local evidence.

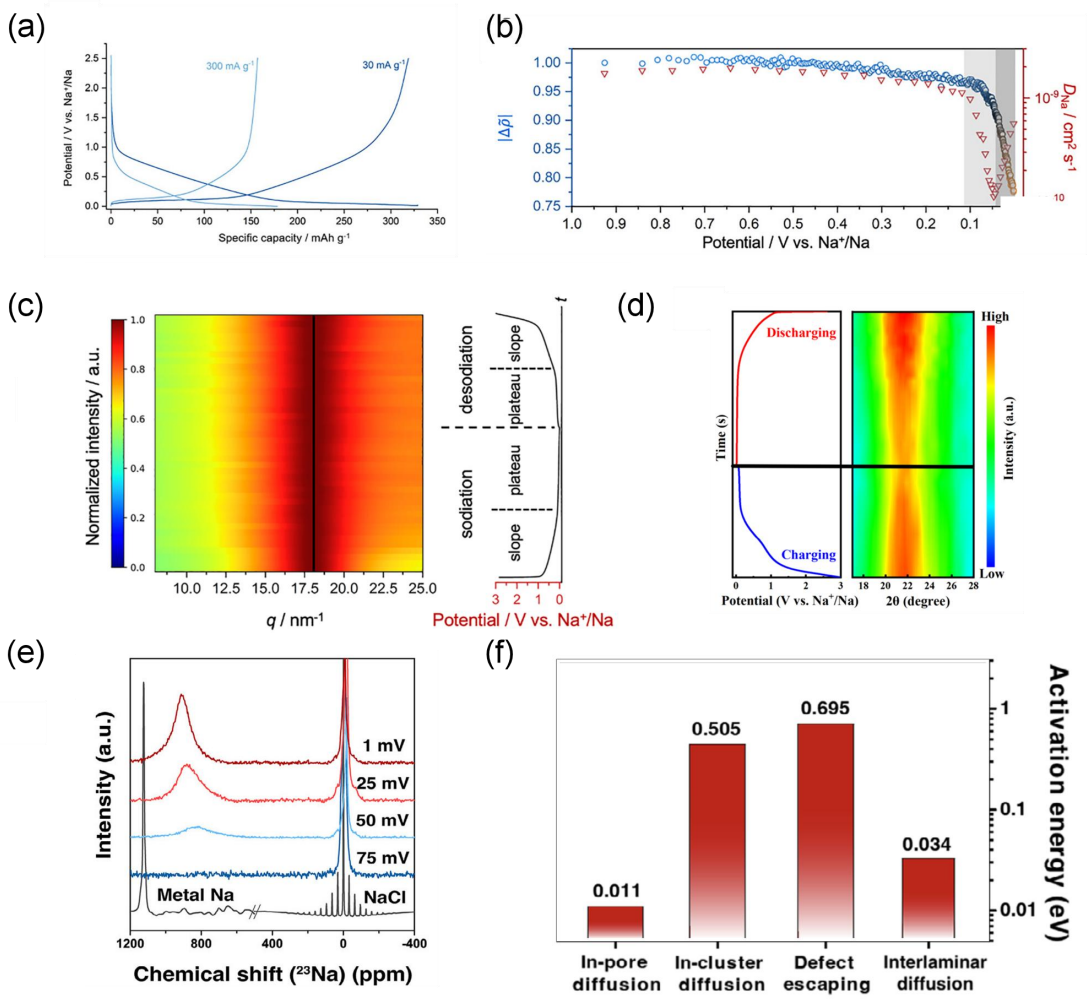


Figure 3. Storage mechanisms and state-dependent kinetics. a, Current-dependent voltage-capacity profiles; b, C(002) response without a resolvable peak shift; c, *In situ* X-ray diffraction (XRD) of pseudo-graphite-dominated hard carbon (PG-HC); d, Scattering-derived electron-density contrast and apparent diffusion derived from the galvanostatic intermittent titration technique (GITT); e, *Ex situ* solid-state ^{23}Na nuclear magnetic resonance (NMR); f, Calculated activation energies in local sodium-carbon environments; cluster self-diffusion includes vacancy formation and migration. Panels a, b and d are from Ref.[5], panel c from Ref.[26], and panels e and f from Ref.[27].

These sites may also host side reactions or trap sodium irreversibly during the first cycle. Lu and colleagues examined resting-induced pre-desolvation before cycling in Na||hard-carbon half-cells containing 1 M $NaPF_6$ in diglyme[8]. Pre-desolvation partially removes

the solvation shell while retaining a solvated sodium environment; presodiation instead replenishes the sodium inventory. First-cycle sodium losses thus involve contributions beyond SEI formation alone. Meaningful ICE comparisons require the electrolyte composition, cutoff potentials and formation conditions to be specified.

Interlayer participation requires material and electrolyte context

The evidence for interlayer storage differs across materials and electrode architectures. Eren and colleagues studied carbon derived from oligomeric 3,4-ethylenedioxythiophene (oligo-EDOT) in cold-pressed electrodes without binders or conductive additives. They observed no resolvable C(002) shift [Figure 3b] and associated the plateau mainly with internal-surface storage and pore filling[5]. Carbon-nanotube-engineered, pseudo-graphite-dominated hard carbon (PG-HC) showed a lower-angle shift of the (002) peak in an ether electrolyte. The shift occurred during sodiation between 0.1 and 0.05 V, indicating interlayer expansion and supporting interlayer participation in this system [Figure 3c][26].

Xiao and colleagues studied hard carbon derived from pre-oxidized phenol-formaldehyde resin and pitch (PFPI-13). They observed layer-peak shifts mainly during the slope, with largely unchanged positions during the plateau[10]. Across these three materials, the interlayer response occurs in different voltage regions or remains unresolved by XRD. Slope and plateau labels therefore provide a starting point for comparison, while local sodium evidence is needed to interpret both shifted peaks and contributions too small to resolve in the average signal. Electrolyte choice adds another source of variation in the storage pathway. Ether-ester comparisons have motivated different interpretations, while a specific ether electrolyte supports low-temperature storage through solvent co-intercalation[28-29]. Solvent participation in this system links pore-entry design directly to the selected electrolyte.

Pore filling and sodium deposition are distinct

Operando SAXS shows sharply reduced electron-density contrast in the late plateau. Over the same region, the apparent diffusion coefficient from the galvanostatic intermittent titration technique (GITT) recovers from its minimum [Figure 3d]. This state-dependent response supports internal pore filling, complemented by wedge-pore studies of reversible storage under confinement[4-5]. The plateau can include contributions

whose relative importance depends on the material. Changing closed-pore dimensions can alter both filling potential and the margin before plating[10]. A higher filling potential may reduce deposition risk while lowering the full-cell voltage. The useful balance depends on the capacity accessible at the operating current. In resin-derived hard carbons tested in sodium hexafluorophosphate/dimethoxyethane electrolyte, Ren and colleagues combined operando diffraction and Raman measurements with calculations to propose coupled intercalation at pore orifices and filling of adjacent cavities[30]. Here, the pore entrance is part of the proposed storage environment as well as an access route to the cavity. This interpretation links pore-entry design to storage-site utilization in the tested resin-derived carbon and electrolyte.

Ex situ solid-state ^{23}Na NMR shows a growing broad signal at large positive chemical shifts during deep sodiation, distinct from the sodium-metal reference. Together with the study's SAXS results, this supports quasi-metallic cluster formation within pores [Figure 3e][27]. Quasi-metallic sodium describes a more metal-like local electronic state within the observed environment. Evaluating surface deposition requires evidence that resolves its location and electrochemical behavior. In full cells, Shan and colleagues combined operando and *ex situ* ^{23}Na NMR to track sodium plating and found that increasing the charge rate shifted its onset to a lower state of charge[31]. Safety assessment therefore combines electrode-potential measurements, tests of reversible sodium removal and suitable plating detection. The usable storage window depends on charging conditions as well as pore structure.

Local migration and electrode rate performance

Comparing kinetic results first requires distinguishing the quantities being measured or calculated. Li and colleagues calculated short-time sodium displacement in a roughly half-filled wedge pore at 600 K over 18 ps. They also suggested that larger pores and greater metallicity may hinder charging and discharging[4]. Lei and colleagues calculated higher activation energies for cluster self-diffusion and defect escape than for in-pore transport and the modeled interlayer pathway [Figure 3f]. The activation energy for cluster self-diffusion includes vacancy formation and migration[27]. Eren and colleagues derived apparent diffusion from the electrode response measured by GITT[5]. These quantities describe short-time motion, rearrangement within occupied clusters and an averaged electrode response, respectively. Comparing them requires the sodium

occupancy, temperature, local configuration and observation time to be specified. Occupancy is a candidate explanation for their different trends, which can be tested by varying it within a common material and electrolyte.

Effective thermodynamic models describe potential-capacity behavior, whereas transport kinetics requires time-dependent evidence[32]. Measured electrode rate performance also depends on the cell configuration used for testing. Overpotential at the sodium counter electrode can trigger premature cutoff, making cell architecture and electrolyte conditions especially important at high loading[33-34]. Separating counter-electrode polarization from the hard-carbon response is therefore an early step in diagnosing underused capacity. Within the hard-carbon electrode, changes in interfacial resistance, pore entry and internal transport can then be compared over the same potential and time range. This diagnosis guides whether functional design should improve access to existing sites, alter the interface or introduce an additional storage phase.

ORGANIZING FUNCTIONAL DESIGN AROUND LIMITING PROCESSES

Transport networks improve utilization of existing sites

Transport-network design targets storage sites that become underused as current increases. Xu and colleagues constructed bicontinuous carbon networks from covalently connected bamboo and carbon-quantum-dot precursors. In their proposed structure, connected graphene nanodomains provide electronic pathways, while surrounding defects and nanocavities support Na adsorption and migration [Figure 4a]. For a representative local path, the defect-edge graphene model containing pyrrolic nitrogen (Npr-G) has a migration barrier of 0.51 eV. The corresponding barrier in the graphene-layer reference model (G-G) is 0.59 eV [Figure 4b]. This barrier difference supports a local transport hypothesis, whose electrode-level contribution depends on the other transport processes[35]. The precursor components undergo carbonization and restructuring, unlike a second phase retained in the final composite. In hard-carbon/MXene composites, two-dimensional transition-metal carbides or nitrides can support conductivity and connections between particles[36].

A useful network must connect particle-scale transport with the behavior of the complete electrode. Graphite-assisted pressurized carbonization combines locally ordered domains with dense, self-supporting fibrous networks, changing both defects and electrode

architecture[38]. Particle-size and loading studies in industrially relevant full cells also show that porous-electrode ionic transport can affect rate performance[39]. Evaluating these networks therefore calls for linking powder conductivity and local migration pathways to electrode measurements at matched loading and compaction density. The relevant gain is improved capacity retention at the intended current and loading after the mass of every component is included.

Active phases introduce additional reaction capacity

Microsized tin-hard-carbon studies assess gravimetric capacity, volumetric capacity and expansion together. Encapsulated tin nanodots offer another way to combine an active phase with a supporting hard-carbon framework[40-41]. Black-phosphorus-hard-carbon studies discuss P-C and P-O-C connections within the composite structure. Subsurface Na_2S_x heterostructures combine active sites, sodium compensation and interfacial modification[42-43]. Measured gains can arise from reactions in the added phase, changes in hard-carbon utilization or altered irreversible sodium loss. Attribution therefore requires the components to be evaluated separately and in combination.

Functional attribution uses individual-component controls to establish reference behavior and compares physical mixtures with deliberately constructed interfaces at matched composition and loading. Mass-weighted component capacity provides a reference, while evidence of interactions between components is needed to establish synergy. Practical benefits can also arise from better contact retention or reduced expansion. The mass of every component, mean desodiation potential and densified electrode volume all enter this evaluation. Accounting for these quantities helps assess how an anode-capacity gain translates into a cell-level energy benefit.

Interfacial layers modify entry and interphase formation

Zhao and colleagues used a metal-organic framework (MOF) glass coating to modify interfacial solvation and transport. Their model contrasts a thicker solvent-derived SEI on bare hard carbon with a thinner NaF-rich interphase on coated hard carbon [Figure 4c]. Arrhenius analysis gives lower apparent activation energies associated with both SEI transport and charge transfer for the coated sample [Figure 4d], supporting improved interfacial kinetics[37]. Artificial SEI layers and few-layer carbon interfaces offer related approaches; the latter also connect solvation changes with interphase formation[44-45].

Their main role is interfacial regulation, distinct from adding a capacity-bearing phase. Lower impedance can reflect changes in desolvation, interphase composition, contact or effective area; separating these contributions helps identify the underlying process. Precursor-derived nitrogen and sulfur doping provides another connection between structural design and interfacial function. In a diglyme electrolyte, Li and colleagues observed a thinner, inorganic-rich SEI and lower fitted interphase resistance for fructose-cysteine-derived hard carbon than for a fructose-only control[46]. The coating and doping examples both connect altered interphase chemistry with improved electrochemical response, but the doping route also changes the carbon framework and pores. Their common design lesson is to evaluate sodium transfer together with interphase formation; the contribution of desolvation remains to be separated from these accompanying changes.

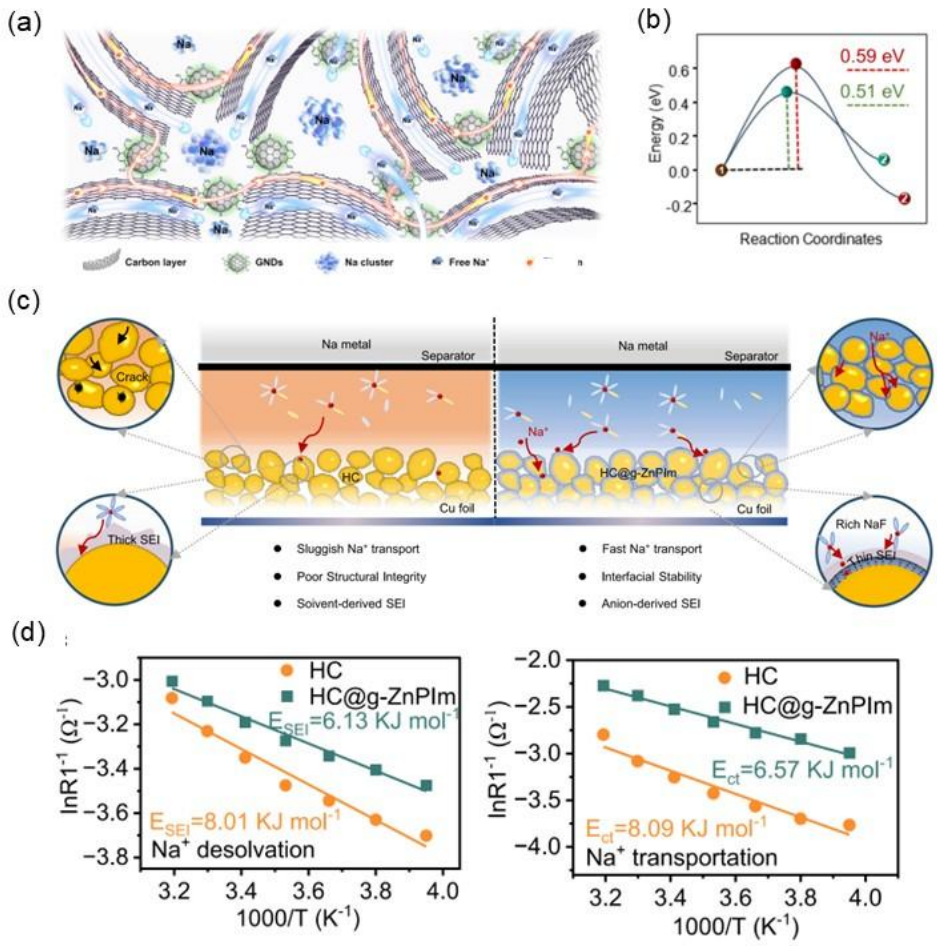


Figure 4. Distinct functions of networks and interfacial coatings. a, Proposed bicontinuous network. GNDs denote the graphene nanodomains shown within the proposed carbon network; b, Local migration barriers of 0.51 and 0.59 eV for the defect-

edge graphene model containing pyrrolic nitrogen (Npr-G) and the graphene-layer reference model (G-G), respectively[35]; c, Interfacial models with and without metal-organic framework (MOF) glass coating. HC denotes hard carbon, and HC@g-ZnPIm is hard carbon coated with melt-quenched ZnPIm glass. The ZnPIm precursor is prepared from zinc oxide, imidazole and phosphoric acid; d, Arrhenius analysis of apparent activation energies associated with solid electrolyte interphase (SEI) transport and charge transfer[37].

Table 1 connects each intervention to the evidence needed to judge its function. A network is evaluated by its effect on reversible utilization at the intended rate, an active phase by its contribution to the complete composite electrode, and an interfacial layer by changes in sodium loss and transfer. In each case, added mass, stability and processing demands determine whether the local improvement remains useful at cell level.

Table 1. Functions of representative designs and priorities for validation.

Intervention and source	Supported interpretation	Contributions to distinguish or validate
Internal pore reconstruction[9]	Scattering, structural characterization and capacity measurements jointly support changes in storage-space utilization	Independent contribution of connectivity at matched pore volume, carbon framework and filling potential
Bicontinuous carbon network[35]	Precursor connectivity and local calculations support the proposed network design	Electrode-level rate performance in relation to local migration barriers, defects and composition
Tin or phosphorus composites[40,42]	Distinct reaction phases operate alongside a hard-carbon framework	Capacity contributions of each component, electrode expansion and additional mass

Intervention and source	Supported interpretation	Contributions to distinguish or validate
Metal-organic framework (MOF) glass interface[37]	Interfacial chemistry and temperature-dependent measurements support changes in sodium entry conditions	Separation of solid electrolyte interphase (SEI), contact and solvation contributions using matched controls
Artificial intelligence (AI)-assisted carbonization[47]	Iterative process optimization has been demonstrated and validated with selected precursors	Predictive range evaluated using independent experiments with new feedstocks, equipment and electrolytes

AI links design variables with validation tasks

The available inputs determine when AI can inform an experiment. Precursor and planned processing variables support pre-synthesis screening, whereas measured structural descriptors support post-synthesis prediction under specified testing conditions. Each task needs an output that can be checked independently. Ji and colleagues investigated temperature-pressure processing spaces, while Liu and colleagues linked composition, processing, structure and performance through staged models[48-49]. Cui and colleagues used machine learning to iteratively optimize carbonization, validating the approach with precursors including cotton, peanut shells and glucose. Another thermal-force-coupled carbonization study also included pouch-cell testing as part of its validation[47,50]. These studies establish a practical role for model-guided processing within their tested ranges. Applying the same approach to another feedstock or furnace introduces a transfer question that can be assessed with independent synthesis and electrochemical tests.

Atomistic models address local storage behavior at a different scale from performance screening. Front and colleagues combined a machine-learning interatomic potential with grand-canonical Monte Carlo sampling of sodium occupancy[51]. The potential approximates atomic energies and interactions, allowing the simulations to generate hypotheses about local storage. Independent structural and local sodium measurements test the proposed storage configurations. New synthesis and cell tests instead assess

predicted processing benefits. Matching each output to its validation endpoint separates local mechanistic interpretation from whole-cell performance prediction.

CONCLUSION AND OUTLOOK

Hard-carbon performance depends on both the formation of sodium-storage sites and their reversible use during cycling. Precursor chemistry and carbonization establish the carbon framework and pore structure, whereas transport and interfacial processes influence how much of that structure contributes to reversible capacity. Electrochemically accessible storage space connects structural characteristics with site utilization under defined electrolyte, potential and time conditions.

Pore filling makes an important contribution to low-potential capacity, while interlayer participation varies with the carbon structure and electrolyte. Measurements of local sodium environments, structural evolution and electrochemical response help distinguish these contributions and their dependence on storage state. At high rates, transport limitations and electrode polarization can leave part of the storage space underused. A larger pore volume is therefore most useful when its additional capacity remains accessible within the charging time and potential margin available. This ties structural design to rate capability, irreversible sodium loss and the voltage retained by the full cell. Functional modification acts on different parts of this process. Conductive networks facilitate charge transport, active phases add reaction capacity, and interfacial layers modify sodium transfer and interphase formation. A capacity gain therefore has different meanings across these designs. Recovering hard-carbon capacity through a network is judged against the transport change, whereas adding a reaction phase requires the entire composite to be assessed. Operating potential, irreversible sodium loss and added mass or volume determine how either gain contributes to full-cell energy.

AI-assisted processing and atomistic modeling contribute at different scales. Process models help select precursors and carbonization conditions, while atomistic models generate testable descriptions of local sodium storage. The resulting design objective is storage space that remains reversibly usable at the intended rate within the cell's sodium inventory and manufacturing constraints. The remaining work is to measure that utilization more directly, establish the net benefit of each modification, and test whether

data-guided choices improve experimental outcomes. These tasks define the three priorities in Figure 5.

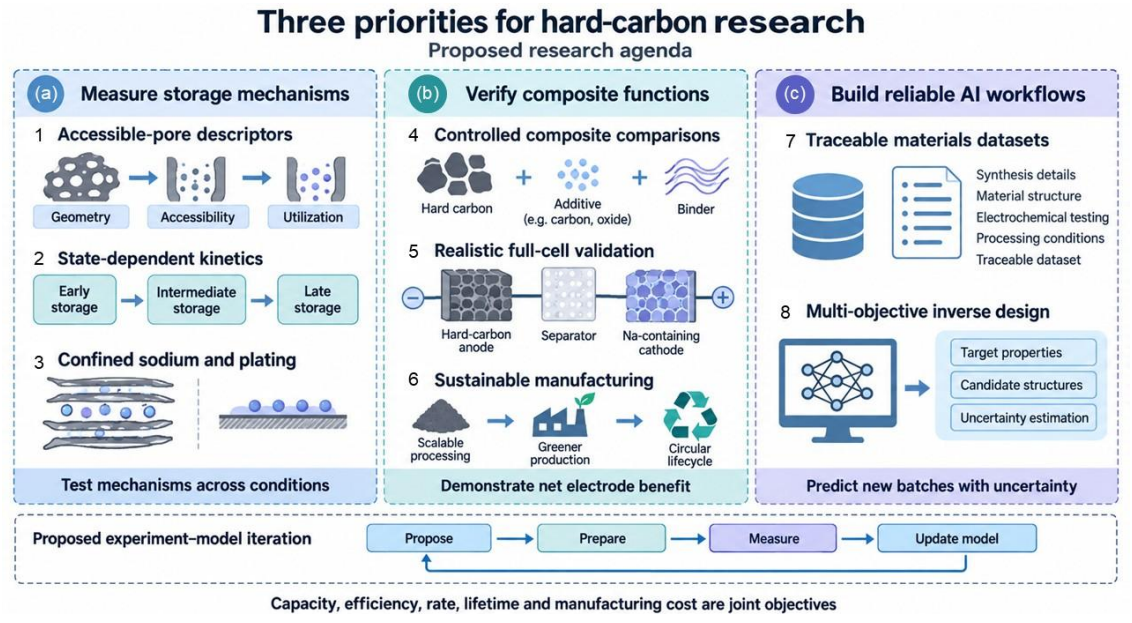


Figure 5. Three priorities and eight research directions. a, Accessible-space descriptors, state-dependent kinetics and discrimination between confinement and deposition; b, Functional controls, realistic-electrode validation and sustainable manufacturing; c, Traceable data and multi-objective inverse design for artificial intelligence (AI)-assisted research. The lower strip builds on existing process iteration to outline further experimental and modeling feedback.

Accessible storage space and state-dependent kinetics

Restricted entry, rearrangement within occupied pores and electrode polarization are competing explanations for rate-dependent capacity loss [Figure 5a]. Accessible-space descriptors should be tested against pore volume or average interlayer spacing for their ability to explain reversible capacity over defined potential and time windows. State-dependent kinetics can be examined by varying occupancy within one material and electrolyte, combining temperature-dependent responses with local sodium measurements. Cross-material comparisons must allow for different occupancies at the same potential. Distinguishing confined sodium from deposition requires their local environments, spatial location and reversible removal to be assessed alongside negative-electrode potential.

These observations should change the intervention chosen. If correcting counter-electrode polarization removes the apparent rate loss, pore redesign becomes a lower priority. If additional low-potential capacity coincides with surface deposition, its assignment to reversible pore utilization needs reassessment.

Functional modification, full-cell performance and sustainable manufacturing

Higher full-cell capacity can reflect added reaction capacity, better hard-carbon utilization or compensation of sodium loss. Functional controls, full-cell validation and manufacturing assessment should distinguish these contributions and their costs [Figure 5b]. Individual-component tests establish reference behavior; physical mixtures and constructed interfaces can then be compared at matched composition and loading. Ampere-hour-scale full-cell examples already provide practical evidence, while dry processing combined with presodiation has addressed finite sodium inventories[4,10,52]. Building on this progress requires batch-to-batch reproducibility, appropriate densification, controlled electrolyte quantities and balanced electrode capacities. Clear energy-density reporting identifies the masses or volumes included in each calculation. Separate reporting of added sodium and intrinsic hard-carbon ICE distinguishes inventory compensation from improved initial reversibility. Net benefits should be reproducible after mass, volume and sodium-inventory costs are included.

Sustainable manufacturing completes this priority by connecting material performance with production demands. Existing scale-up and techno-economic studies provide a basis for assessing precursor variability, carbon yield, thermal processing and washing together[53]. Life-cycle analysis identifies pyrolysis energy as an important burden at laboratory scale. Prospective models explore the effects of emissions, argon and acid use under larger-scale production scenarios[54]. Measured yields and material and energy flows can test these scenarios. Poor yield or intensive thermal treatment may outweigh a laboratory capacity gain, requiring production routes to be compared within explicit system boundaries, including for biomass-derived precursors.

Data-driven design and experimental feedback

Models may learn testing or publication differences alongside material effects, linking the need for traceable data with independent validation [Figure 5c]. Records should connect synthesis, measured structure, testing and outcomes while retaining batch

identities, replicates and unsuccessful experiments. Measured and estimated descriptors need distinct labels, and inputs must be available at the intended prediction stage. Related sample or publication records should remain together during data splitting. Tests on new batches, precursors or equipment assess reliability with uncertainty reported. Feature importance identifies relationships for controlled testing.

Multi-objective inverse design selects conditions against explicit application targets, keeping trade-offs among capacity, ICE, plateau-rate capability, lifetime and manufacturing demands visible. Active learning can select experiments to improve performance or distinguish between uncertain predictions. Demonstrated process iteration offers a starting point, while transferring capacity-ICE relationships across systems requires external validation.[47] Equal experimental budgets allow comparison with random or empirical screening through independently confirmed candidates and experiments needed to resolve a design uncertainty. Failure on a new precursor family or furnace should guide additional measurements or a narrower application range. These endpoints test whether predictive accuracy translates into better experimental choices.

DECLARATIONS

Authors' contributions

Curated and analyzed the literature, prepared the figures, and wrote the original draft: Xue PC;

Contributed to literature curation and analysis and reviewed and edited the manuscript: Hu HY, Huang HY, Wu YT, Chen Z, Zeng ZY, Zhong XY;

Contributed to the conceptualization and supervision of the work, acquired funding, and reviewed and edited the manuscript: Han MS;

All authors discussed the content and approved the final version of the manuscript.

Availability of data and materials

This review is based on published literature. No original experimental or computational datasets are reported in this article. The published sources supporting the discussion are cited in the reference list.

AI and AI-assisted tools statement

Generative artificial intelligence (AI) tools accessed through Codex (OpenAI) were used to create the individual graphical elements for Figures 1 and 5 and the table-of-contents graphic. The AI tool did not influence the study design, data collection, analysis, interpretation, or the scientific content of the work. All authors take full responsibility for the accuracy, integrity, and final content of the manuscript.

Financial support and sponsorship

This work was financially supported by Guangdong Major Project of Basic and Applied Basic Research (2023B0303000002), Key Projects of the National Natural Science Foundation of China (No. 52536003), and High level of special funds (G03034K001).

Conflicts of interest

All authors declared that there are no conflicts of interest.

Ethical approval and consent to participate

Not applicable.

Consent for publication

Not applicable.

Copyright

© The Author(s) 2026.

REFERENCES

[1] A. Yao, S. M. Benson, W. C. Chueh, Critically assessing sodium-ion technology roadmaps and scenarios for techno-economic competitiveness against lithium-ion batteries, *Nat. Energy* **2025**, 10, 404,[DOI: 10.1038/s41560-024-01701-9]

[2] C. Vaalma, D. Buchholz, M. Weil, S. Passerini, A cost and resource analysis of sodium-ion batteries, *Nature Reviews Materials* **2018**, 3, 18013,[DOI: 10.1038/natrevmats.2018.13]

[3] Y. Liu, B. V. Merinov, W. A. Goddard, III, Origin of low sodium capacity in graphite and generally weak substrate binding of Na and Mg among alkali and alkaline earth

metals, *Proceedings of the National Academy of Sciences* **2016**, 113, 3735,[DOI: 10.1073/pnas.1602473113]

[4] Y. Li, A. Vasileiadis, Q. Zhou, et al., Origin of fast charging in hard carbon anodes, *Nat. Energy* **2024**, 9, 134,[DOI: 10.1038/s41560-023-01414-5]

[5] E. O. Eren, E. Senokos, E. Scoppola, Z. Song, M. Antonietti, P. Giusto, An enhanced three-stage model for sodium storage in hard carbons, *Energy Environ. Sci* **2025**, 18, 7859,[DOI: 10.1039/D4EE06029F]

[6] J. Lin, Q. Zhou, Z. Liao, et al., Steric Hindrance Engineering to Modulate the Closed Pores Formation of Polymer-Derived Hard Carbon for High-Performance Sodium-Ion Batteries, *Angew. Chem. Int. Ed.* **2024**, 63, e202409906,[DOI: 10.1002/anie.202409906]

[7] Z. Xu, J. Wang, Z. Guo, et al., The Role of Hydrothermal Carbonization in Sustainable Sodium-Ion Battery Anodes, *Adv. Energy Mater.* **2022**, 12, 2200208,[DOI: 10.1002/aenm.202200208]

[8] Z. Lu, H. Yang, Y. Guo, et al., Consummating ion desolvation in hard carbon anodes for reversible sodium storage, *Nat. Commun.* **2024**, 15, 3497,[DOI: 10.1038/s41467-024-47522-y]

[9] G. Jin, C. Wang, F. Jin, et al., Interconnected Closed Pores Enable Dense and Facile Sodium Storage in Hard Carbon, *Adv. Mater.* **2026**, 38, e74503,[DOI: 10.1002/adma.74503]

[10] S. Xiao, Y.-J. Guo, H.-X. Chen, et al., Insight into the Role of Closed-Pore Size on Rate Capability of Hard Carbon for Fast-Charging Sodium-Ion Batteries, *Adv. Mater.* **2025**, 37, 2501434,[DOI: 10.1002/adma.202501434]

[11] C. Wu, Y. Yang, Y. Zhang, et al., Hard carbon for sodium-ion batteries: progress, strategies and future perspective, *Chem. Sci.* **2024**, 15, 6244,[DOI: 10.1039/D4SC00734D]

[12] C. Matei Ghimbeu, A. Beda, B. Réty, et al., Review: Insights on Hard Carbon Materials for Sodium-Ion Batteries (SIBs): Synthesis - Properties - Performance Relationships, *Adv. Energy Mater.* **2024**, 14, 2303833,[DOI: 10.1002/aenm.202303833]

[13] X. Chen, C. Liu, Y. Fang, et al., Understanding of the sodium storage mechanism in hard carbon anodes, *Carbon Energy* **2022**, 4, 1133,[DOI: 10.1002/cey2.196]

[14] Z. Tang, R. Zhang, H. Wang, et al., Revealing the closed pore formation of waste wood-derived hard carbon for advanced sodium-ion battery, *Nat. Commun.* **2023**, 14, 6024,[DOI: 10.1038/s41467-023-39637-5]

[15] Y. Wang, Z. Yi, L. Xie, et al., Releasing Free Radicals in Precursor Triggers the Formation of Closed Pores in Hard Carbon for Sodium-Ion Batteries, *Adv. Mater.* **2024**, 36, 2401249,[DOI: 10.1002/adma.202401249]

[16] Z. Wen, R. Zhao, T. Tian, et al., Molecular Stitching in Polysaccharide Precursor for Fabricating Hard Carbon with Ultra-High Plateau Capacity of Sodium Storage, *Adv. Mater.* **2025**, 37, 2420251,[DOI: 10.1002/adma.202420251]

[17] J. Liu, Y. You, L. Huang, et al., Precisely Tunable Instantaneous Carbon Rearrangement Enables Low-Working-Potential Hard Carbon Toward Sodium-Ion Batteries with Enhanced Energy Density, *Adv. Mater.* **2024**, 36, 2407369,[DOI: 10.1002/adma.202407369]

[18] W. Jia, Z. Cui, S. Zhao, et al., Liquid-Phase Spatial Confinement Engineering of sp2-Rich Closed-Pore Hard Carbon for Sodium-Ion Batteries, *Adv. Energy Mater.* **2026**, e71369,[DOI: 10.1002/aenm.71369]

[19] W.-Y. Qian, X.-Y. Zhou, X.-Y. Liu, M.-Y. Su, K.-Y. Zhang, X.-L. Wu, Breakage of the dense structure of coal precursors increases the plateau capacity of hard carbon for sodium storage, *Chem. Sci.* **2025**, 16, 104,[DOI: 10.1039/d4sc06549b]

[20] Y. Zhang, S.-W. Zhang, Y. Chu, et al., Redefining closed pores in carbons by solvation structures for enhanced sodium storage, *Nat. Commun.* **2025**, 16, 3634,[DOI: 10.1038/s41467-025-59022-8]

[21] J. M. Stratford, A. K. Kleppe, D. S. Keeble, et al., Correlating Local Structure and Sodium Storage in Hard Carbon Anodes: Insights from Pair Distribution Function Analysis and Solid-State NMR, *J. Am. Chem. Soc.* **2021**, 143, 14274,[DOI: 10.1021/jacs.1c06058]

[22] J. M. Stratford, P. K. Allan, O. Pecher, P. A. Chater, C. P. Grey, Mechanistic insights into sodium storage in hard carbon anodes using local structure probes, *Chem. Commun.* **2016**, 52, 12430,[DOI: 10.1039/c6cc06990h]

[23] R. Morita, K. Gotoh, M. Fukunishi, et al., Combination of solid state NMR and DFT calculation to elucidate the state of sodium in hard carbon electrodes, *J. Mater. Chem. A* **2016**, 4, 13183,[DOI: 10.1039/c6ta04273b]

[24] B. Wang, J. R. Fitzpatrick, A. Brookfield, et al., Electron paramagnetic resonance as a tool to determine the sodium charge storage mechanism of hard carbon, *Nat. Commun.* **2024**, 15, 3013,[DOI: 10.1038/s41467-024-45460-3]

[25] Y. Chen, G. Liu, Y. Zhao, et al., Atomic-Level Insight of Carbon-Based Anodes for Advanced Sodium Storage: Electrochemical Mechanisms and Molecular Simulation-Assisted Modification, *cMat* **2026**, 3, e70042,[DOI: 10.1002/cmt2.70042]

[26] H. Yu, X. Liu, Z. Zhang, et al., Engineering Pseudo-Graphite-Dominated Hard Carbon as Anode for Sodium-Ion Batteries, *ACS Energy Letters* **2025**, 10, 4342,[DOI: 10.1021/acsenergylett.5c01780]

[27] Z.-Q. Lei, S.-H. Xiao, Z. Ran, et al., Circumventing Self-Diffusion Enables High-Rate Hard Carbon Anodes, *Adv. Mater.* **2026**, 38, e13193,[DOI: 10.1002/adma.202513193]

[28] G. Liu, Z. Wang, H. Yuan, et al., Deciphering Electrolyte Dominated Na^+ Storage Mechanisms in Hard Carbon Anodes for Sodium-Ion Batteries, *Adv. Sci.* **2023**, 10, 2305414,[DOI: 10.1002/advs.202305414]

[29] M. Li, Z. Liu, Y. Zhao, Z. Chen, Y. Zhang, N. Zhang, Enhanced sodium storage in hard carbon via solvent co-intercalation electrolyte enabling Ah-level pouch cells at low temperatures, *Nat. Commun.* **2026**, 17, 1478,[DOI: 10.1038/s41467-026-69237-y]

[30] R. Ren, L. Zhang, J. Zhu, et al., Nano-Space Confinement Drives Rational Closed Pore Design in Hard Carbons for High-Capacity and High-Rate Sodium Storage, *Nano-Micro Letters* **2026**, 18, 382,[DOI: 10.1007/s40820-026-02223-7]

[31] P. Shan, W. Wu, H. Zhang, et al., Quantitative tracking of sodium plating in hard carbon anodes, *eScience* **2026**, 100649,[DOI: 10.1016/j.esci.2026.100649]

[32] H. S. Nguyen, A. Latz, An effective model for sodium insertion in hard carbons, *Physical Chemistry Chemical Physics* **2023**, 25, 28196,[DOI: 10.1039/d3cp03186a]

[33] Z. Li, Z. Jian, X. Wang, I. A. Rodríguez-Pérez, C. Bommier, X. Ji, Hard carbon anodes of sodium-ion batteries: undervalued rate capability, *Chem. Commun.* **2017**, 53, 2610,[DOI: 10.1039/c7cc00301c]

[34] C. Müller, Z. Wang, A. Hofmann, et al., Influences on Reliable Capacity Measurements of Hard Carbon in Highly Loaded Electrodes, *Batteries & Supercaps* **2023**, 6, e202300322,[DOI: 10.1002/batt.202300322]

[35] L.-Z. Xu, J.-X. Chen, D.-G. Liu, et al., Covalent Quantum Bridging Enables Bicontinuous Electron-Ion Highways in Hard Carbon for Ultrafast Sodium Storage, *J. Am. Chem. Soc.* **2026**, 148, 12849,[DOI: 10.1021/jacs.5c21030]

[36] H.-l. Cao, L.-t. Yang, M. Zhao, et al., A flexible hard carbon microsphere/MXene film as a high-performance anode for sodium-ion storage, *New Carbon Materials* **2022**, 37, 1154,[DOI: 10.1016/s1872-5805(22)60616-4]

[37] J. Zhao, W. Yang, Y. Fan, Z. Chang, H. Zhou, Metal-organic framework glass enables durable sodium-ion storage for hard carbon negative electrodes, *Nat. Commun.* **2026**, 17, 8287,[DOI: 10.1038/s41467-026-75060-2]

[38] Y. Du, Y. Qiu, R. Zhuang, et al., Superior initial Coulombic efficiency and areal capacity of hard carbon anode enabled by graphite-assisted carbonization for sodium-ion battery, *Carbon* **2024**, 221, 118929,[DOI: 10.1016/j.carbon.2024.118929]

[39] C. Constable, F. Coowar, M. Copley, E. Kendrick, C. Dancer, I. Hasa, Influence of Particle Size and Mass Loading of Hard Carbon on Sodium Ion Battery Rate Performance in Industrially Relevant Full Cells, *J. Electrochem. Soc.* **2024**, 171, 023506,[DOI: 10.1149/1945-7111/ad2590]

[40] X. Gao, Z. Yan, L. Lin, et al., Microsized Sn-Hard Carbon Composite Anode with Capacities of 583 mAh g^{-1} and 1,073 mAh cm^{-3} for Sodium-Ion Batteries, *ACS Energy Letters* **2026**, 11, 1916,[DOI: 10.1021/acsenergylett.5c03621]

[41] S. Choi, D.-Y. Han, T. Bok, et al., Catalytic Tin Nanodots in Hard Carbon Structures for Enhanced Volumetric and Power Density Batteries, *ACS Nano* **2025**, 19, 10476,[DOI: 10.1021/acsnano.5c00528]

[42] W. Ai, L. Li, S. Dong, et al., High-performance sodium-ion anode based on stable phosphorus-carbon bond in black phosphorus−hard carbon nanocomposite, *J. Power Sources* **2024**, 618, 235211,[DOI: 10.1016/j.jpowsour.2024.235211]

[43] Y. Huang, H. Yang, Z. Zheng, et al., A facile graft-repair strategy: Subsurface Na2Sx heterostructures in hard carbon anodes for high-capacity and ultrafast sodium-ion storage, *Carbon* **2024**, 221, 118922,[DOI: 10.1016/j.carbon.2024.118922]

[44] L. Shi, Y. Sun, W. Liu, et al., Pre-engineering artificial solid electrolyte interphase for hard carbon anodes for superior sodium storage performance, *Chem. Commun.* **2023**, 59, 12723,[DOI: 10.1039/d3cc03967f]

[45] S. Zhao, F. Huang, Weakly Solvating Few-Layer-Carbon Interface toward High Initial Coulombic Efficiency and Cyclability Hard Carbon Anodes, *ACS Nano* **2024**, 18, 1733, [DOI: 10.1021/acsnano.3c11171]

[46] H. Li, Y. Zhou, Y. Yang, et al., Manipulating Interphase Chemistry by Endogenous Doping Toward High-Performance Hard Carbon Anodes for Sodium-Ion Batteries, *Nano-Micro Letters* **2026**, 18, 276,[DOI: 10.1007/s40820-026-02124-9]

[47] J. Cui, Y. Rao, J. Gao, et al., Data-driven intelligent carbonization unifies diverse biomass into high-performance hard carbon negative electrodes, *Nat. Commun.* **2026**, 17, 3885,[DOI: 10.1038/s41467-026-70411-5]

[48] T. Ji, X. Liu, D. Sheng, et al., Machine learning-assisted thermomechanical coupling fabrication of hard carbon for sodium-ion batteries, *Energy Stor. Mater.* **2024**, 71, 103563,[DOI: 10.1016/j.ensm.2024.103563]

[49] M. Liu, Q. Tang, E. Leng, Y. Deng, D. Lv, J. E, Multi-staged machine learning-driven investigation of biomass-derived hard carbon anodes for sodium-ion batteries: Connecting precursor, structure, and performance, *Chem. Eng. J.* **2026**, 528, 172350,[DOI: 10.1016/j.cej.2025.172350]

[50] Z. Sun, H. Liu, Y. Cheng, et al., 900 °C thermal-force coupling carbonization tailoring hard carbon microstructures enables high performance sodium-ion pouch batteries, *Nat. Commun.* **2026**,[DOI: 10.1038/s41467-026-77440-0]

[51] A. Front, T. Ala-Nissilä, M. A. Caro, Density-dependent sodium-storage mechanisms in hard carbon materials, *Chem. Sci.* **2026**, 17, 9570,[DOI: 10.1039/d6sc00030d]

[52] N. Qin, Y. Li, H. Yang, et al., Integrating dry-processing and pre-sodiation enables high-energy sodium ion batteries, *Nat. Commun.* **2025**, 16, 11474,[DOI: 10.1038/s41467-025-66492-3]

[53] Z. Guo, K. Zheng, M. Wang, et al., Sustainable Hard Carbon as Anode Materials for Na-Ion Batteries: From Laboratory to Upscaling, *Batteries & Supercaps* **2025**, 8, e202400428,[DOI: 10.1002/batt.202400428]

[54] H. Liu, M. Baumann, H. Moon, et al., Life cycle assessment of bio-based hard carbon for sodium-ion batteries across different production scales, *Chem. Eng. J.* **2024**, 495, 153410,[DOI: 10.1016/j.cej.2024.153410]